frontiers | Frontiers in Marine Science

TYPE Original Research
PUBLISHED 21 October 2022
DOI 10.3389/fmars.2022.1028052



OPEN ACCESS

EDITED BY
Yuan Lin,
Zhejiang University, China

REVIEWED BY
Paul Yancey,
Whitman College, United States
Junichi Miyazaki,
Japan Agency for Marine-Earth Science and Technology (JAMSTEC), Japan
Haocai Huang,
Zhejiang University, China

*CORRESPONDENCE
Yongping Jin
jinyongping@hnust.edu.cn

SPECIALTY SECTION
This article was submitted to Ocean Observation, a section of the journal Frontiers in Marine Science

RECEIVED 25 August 2022
ACCEPTED 10 October 2022
PUBLISHED 21 October 2022

CITATION
Liu G, Jin Y, Peng Y, Liu D and Wan B (2022) A novel active deep-sea low-damage pressure-retaining organisms sampler.
*Front. Mar. Sci.* 9:1028052.
doi: 10.3389/fmars.2022.1028052



# A novel active deep-sea low-damage pressure-retaining organisms sampler

Guangping Liu, Yongping Jin*, Youduo Peng, Deshun Liu and Buyan Wan

National-Local Joint Engineering Laboratory of Marine Mineral Resources Exploration Equipment and Safety Technology, Hunan University of Science and Technology, Xiangtan Hunan, China

Capturing less damaged organisms samples is the basis for research on the biological communities, living environments, biological life compositions, and biological tissue structures of organisms livinin the deep seabed. The hadal snailfish is pressure-tolerant, cold-tolerant, and easily damaged. This research used a hydraulic suction macro-biological pressure-retaining sampler (HSMPS) to capture less damaged hadal snailfish samples *via* pumping. As the hadal snailfish is sucked into the macro-organism pressure-maintaining sampler, it inevitably collides with the suction pipe in the diversion area (SPDA) and the inner wall of the pressure-maintaining cylinder in the pressure-maintaining area (PCPA). Therefore, a finite element analysis model of a hadal snailfish with a real geometric shape was constructed by obtaining the material mechanical properties of different parts of the fish on the seabed through static compression tests, and the dynamic modeling and response analysis of the hadal snailfish during the capture process was carried out. Moreover, the dynamic response changes of the stress, strain and acceleration of various tissues and organs of the hadal snailfish during the capture process were determined, thereby providing technical support for the research and development of marine biological sampling equipment.

KEYWORDS

**deep sea environment, pressure-retaining sampling, low-damage sampling, dynamic response analysis, Hadal snailfish**

## Introduction

There are many kinds of biological resources and new biological species in the abyss. Obtaining active samples from the abyss is the premise of scientific research on its environmental changes, life evolution process, macro-organism species distribution, and living conditions. (Jamieson et al., 2010; Ramirez-Llodra et al., 2010; Clark et al., 2016). The deep seabed is characterized by ultra-high pressure and low temperatures; thus, current biological samplers complete the process of collecting benthic organisms in the

abyss and then returning to the surface. Due to the influence of the decrease of the external pressure and the increase of the external temperature of the biological sampler, the collected organisms are killed, which has a significant impact on the proper research of the living conditions of the organisms in this seabed area and the seabed environment (Caron et al., 2015; Edgcomb et al., 2016; Feng et al., 2020).

The hadal snailfish is considered to be the deepest-dwelling vertebrate on earth. Its living environment is extreme and is characterized by high hydrostatic pressure, low temperatures, hypoxia, and high salt. Thus, the hadal snailfish is characterized by pressure resistance, temperature resistance, and easy damage. Some scholars have researched deep-sea pressure and heat preservation sampling, but there has been no report on the dynamic response analysis of deep-sea organisms during the sampling process. However, the dynamic responses of the tissues and organs of deep-sea organisms during the sampling process are the key factors affecting biological activity (Billings et al., 2017; Garel et al., 2019; Peoples et al., 2019; Wang et al., 2020). Because the hadal snailfish lives in the extreme environment of the deep sea, its dynamic response during the capture process cannot be analyzed in a laboratory. The development of advanced numerical and computational techniques makes it possible to perform the dynamic response analysis of the hadal snailfish during its capture. Compared with the experimental method, the numerical method provides a more cost-effective approach to obtaining the eventual outcomes, as well as the behaviors, of different tissues and organs of the hadal snailfish and has been widely used in the study of fish collision problems. As shown in Figure 1, the Fendouzhe manned submersible was carried on the Tan Suo Yi Hao scientific research ship to catch hadal snailfish on the seabed at a depth of 7,731 m. Because there is no pressure-retaining device in this sampling process, the hadal snailfish cannot survive in the recovery process of the sampler. The head of the hadal snailfish sample we caught this time showed signs of injuries, but it was not sure whether these injuries affected the survival of the hadal snailfish. However, Gerringer et al. (2017) pointed out that the pores on the head of hadal snailfish are easily damaged or lost during sampling and recovery and that the fragile skin has been damaged to the extent that the temporal cephalic pores are lost, making it impossible to determine which genus a specimen should be assigned.

For deep-sea organisms sampling, samplers are mainly mounted on remotely operated vehicles and submersibles to collect samples of interest by passive trapping. In deep-sea organisms' low damage sampling, Billings et al. (2017) developed a SyPRID sampler, which operated at a depth of 6000m, using perforated ultra-high molecular weight (UHMW) plastic tubes, supporting a fine mesh in the outer carbon composite tube (tube in tube design), and installing an axial flow pump at the end of the capture filter. They completed sampling at 2160m on the seafloor. With the increasing demand for deep-sea organisms sampling, Phillips et al. (2019) developed a soft robotic arm to protect vulnerable deep-sea organisms samples by controlling a wearable glove gripper (made of materials compatible with the soft and fragile nature of marine organisms) to perform sampling operations in 2300 m water depth. Vogt et al. (2018) used additive manufacturing of flexible materials to obtain a flexible palm grip, improving the operational stability of the soft manipulator by adding interactive "nails" to the soft fingertips for flexible gripping of samples on rigid substrates. At present, organisms sampling for

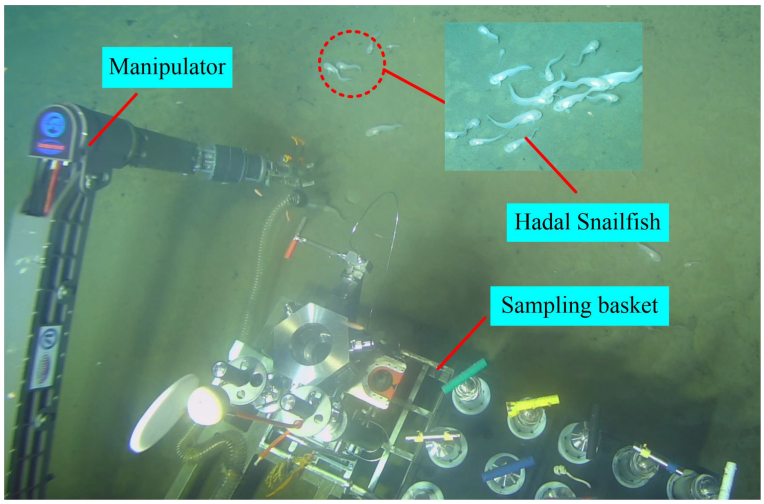


FIGURE 1
Fendouzhe manned submersible catches hadal snailfish.

the seafloor above 3000 m is done using samplers, and although much work has been done on pressure-retaining, the dynamic response of organisms during sampling has not been reported. However, some gelatinous fish are in the deep-sea environment, and it is easy to damage them during the collection process. Marine biologists have tried to catch megafaunal organisms without damaging them for decades, using traditional hard-bodied robotic hands or claws. However, it has only been applied at a depth of about 2000m on the seafloor, can only catch organisms with weak mobility, and is not designed to retain pressure, which is an essential factor affecting the activity of deep-sea organisms. Therefore, we propose a low-damage Pressure-retaining organisms sampling method to meet the demand for high-quality organisms samples for marine scientific research.

This work is based on a hydraulic suction macro-biological pressure sampler (HSMPS), in which a suction pump generates negative pressure to capture benthic organisms. Taking the hadal snailfish as the research object, according to its scanning and anatomical data, a finite element model of the hadal snailfish with real geometry was constructed. The dynamic modeling and response analysis of the capture process of the hadal snailfish were carried out, and the dynamic response changes of the stress, strainand acceleration of various tissues and organs during the capture process were determined. The findings provide technical support for the structural design of deep-sea biological sampling equipment and the life evolution of deep-sea biological communities.

## Hydraulic suction macro-biological pressure sampler

Deep-sea organisms live in the high-pressure and low-temperature environment of the seabed for a long time. To obtain *in-situ* biological samples from the seabed, it is necessary to develop a set of marine biological equipment. Marine biological sampling equipment currently solves the problems of pressure and heat preservation, but there is no research on the dynamic response of the deep-sea biological capture process. Some soft and highly fragile organisms live in the deep sea, and it is easy for the sampler to cause damage to these organisms in the sampling process. Therefore, this paper designs a deep-sea low-damage and pressure-keeping biological sampler.

The structure of HSMPS is shown in Figure 2, which includes three parts: diversion area, pressure-maintaining area and pumping area. HSMPS can be carried on manned or unmanned submersibles for operation. The suction pump in the pumping area generates negative pressure, so that the fish-water mixture enters the pressure-maintaining area through the diversion area. The pressure-maintaining area is provided with a

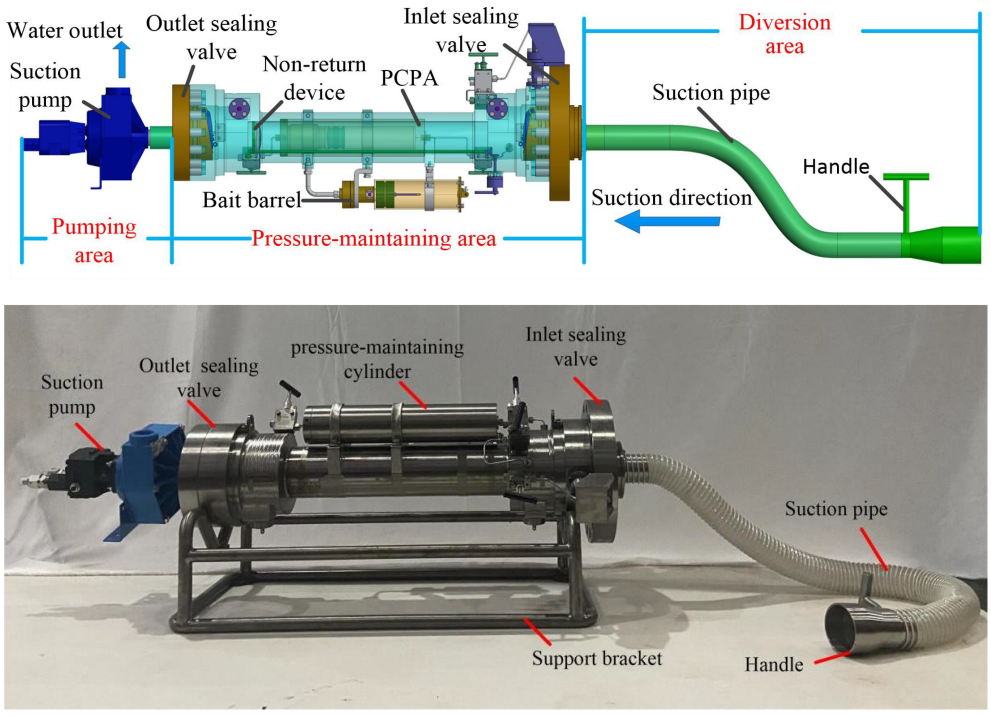


FIGURE 2
Structure of HSMPS.

check valve to prevent the hadal snailfish from being sucked into the pumping area. The pressure-maintaining area includes a pressure-maintaining cylinder, a pressure compensator and a bait cylinder. The function of the pressure-maintaining cylinder is to provide a high-pressure environment for deep-sea organisms. The pressure-maintaining cylinder can bear the pressure of 110MPa, and is made of TC4 titanium alloy, which has the characteristics of high strength, light weight and corrosion resistance. The inner diameter of the pressure-maintaining cylinder is 68mm and the length is 526 mm. During the recovery process of the sampler, the pressure difference between inside and outside will cause the deformation of the pressure-maintaining cylinder, which will lead to the pressure change in the pressure-maintaining cylinder. The function of the pressure compensator is to compensate the pressure drop caused by the expansion and deformation of the pressure-maintaining cylinder. The purpose of bait is to provide nutrients for deep-sea organisms. We will wrap a layer of thermal insulation material on the outer wall of the pressure-maintaining cylinder, so as to prevent the temperature change from affecting the deep-sea organisms in the recovery process of the sampler. The diversion area includes a suction pipe and a handle, the suction pipe is a flexible hose, the suction pipe is connected with the handle through a clamp, and the submarine operator can manipulate the manipulator to grab the handle to capture the benthic organisms, and the inner wall of the suction pipe is made of rubber material. The pump suction area includes a suction pump and a hydraulic pipeline. The suction pump is connected with the hydraulic source on the submersible through the hydraulic pipeline, and the flow rate of the suction pump can be adjusted. Xu et al. (2018) pointed out that when the flow rate of the suction pump is higher than the limit flow rate of fish, the fish can't continue to swim upstream, but the limit flow rate of fish is in the range of 0.6m/s ~ 1.2m/s. However, the excessive suction flow of the suction pump can easily cause damage to the deep-sea organisms, while the too small suction flow can't suck the deep-sea organisms. Therefore, the maximum suction flow of the suction pump is 18$m^3$/h.

The work of HSMPS is divided into three processes: lowering, capturing, and recycling and the work process of HSMPS is shown in Figure 3. Deep-sea organisms inevitably collide with the suction tube in the diversion area (SPDA) and the inner wall of the pressure-maintaining cylinder in the pressure-maintaining area (PCPA) during the process of being captured, which is very likely to cause damage to deep-sea organisms during the collision. Therefore, we take the hadal snailfish, a species unique to the abyss, as the research object and carry out the dynamics modeling and response analysis of the

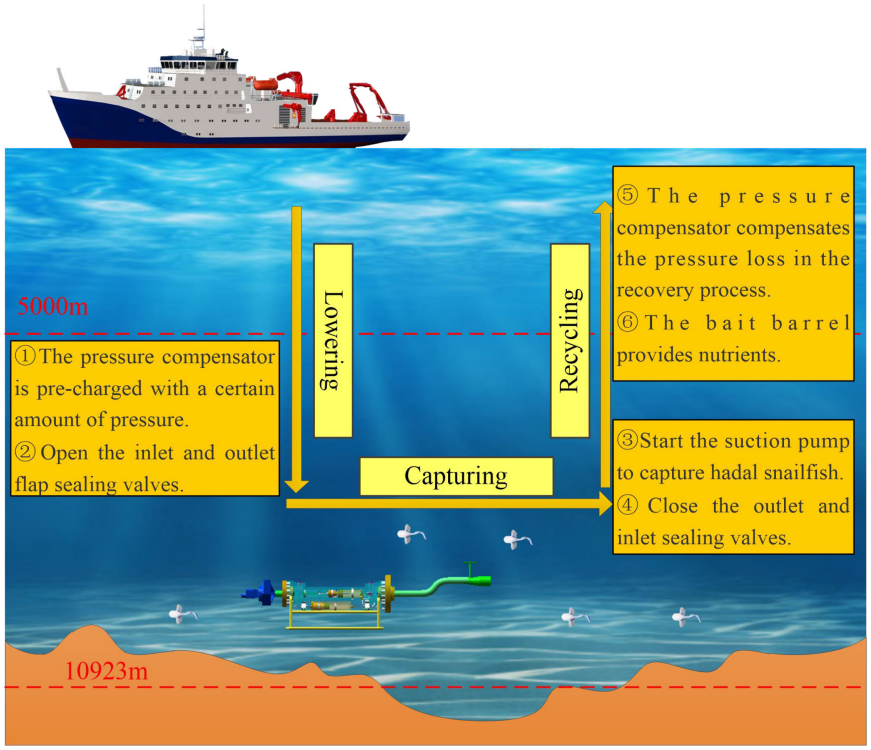


FIGURE 3
Working process of HSMPS.

capture process of the hadal snailfish by establishing the finite element analysis model of the hadal snailfish to determine the dynamic response changes of stress, strain, and acceleration of each tissue and organ of the hadal snailfish during the capture process.

## Materials and models

### Three-dimensional model of the hadal snailfish

As shown in Figure 4, the model construction of the hadal snailfish was divided into the following four steps: entity data acquisition, 3D model construction, point cloud data processing, and precise surface processing.

### Entity data acquisition

According to the scanning and anatomical data of the hadal snailfish, the distribution and geometric data of its various tissues and organs were obtained, as shown in Figures 4A, B. The hadal snailfish sample was captured by the manned submersible Fendouzhe at a depth of 7,731 m in the Western Philippine Basin. Hadal snailfish tissues and organs are composed of bone tissue and soft tissue, among which the bone tissue includes the skull, frontal bone, vertebrae, and fins, while the soft tissue includes the gills, liver, stomach, eggs, back muscles, and skin. The body of the hadal snailfish is elongated with a length between 160 and 200 mm, and the widest part of the body is 45 mm. The front part of the body is sub-cylindrical, the back part is gradually flat and narrow, and the outline of the body has symmetrical geometry. The skin is only a very thin layer of membrane; thus, the physiological tissues in the hadal

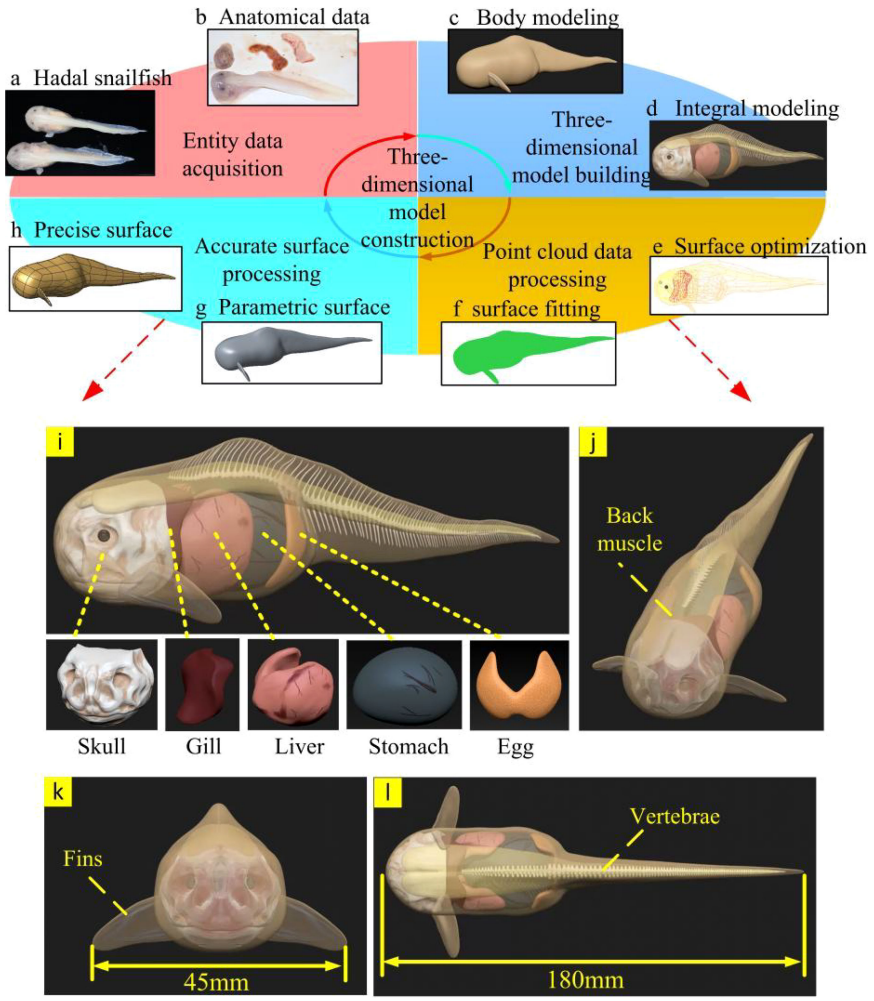


FIGURE 4
Modeling process and structure of tissues and organs of hadal snailfish **(A–H)** construction of a 3D model of hadal snailfish; **(I)** tissue and organ distribution of hadal snailfish; **(J–L)** three views of hadal snailfish.

snailfish can fill with water, the internal and external pressure can be balanced, and there are no scales. The skull of the hadal snailfish, which is wide and flat, is located directly in front of the body, and the skull is not completely closed. To adapt to the high-pressure environment, its bones are very thin and have the ability to bend. The fins of the hadal snailfish are symmetrically distributed on both sides of the body, its gills are located behind the skull, its liver is adjacent to the gills, and behind the liver is the swollen stomach. *Via* anatomical observation, a large number of crustaceans with relatively complete shapes have been found in the stomach contents of hadal snailfish, and its eggs are located behind the stomach. The back muscles and vertebrae are located above the body (Yancey et al., 2014; Linley et al., 2016; Gerringer et al., 2017; Linley et al., 2017; Wang et al., 2019; Orr, 2020).

### Three-dimensional model building

Polygon and curved surface modeling are used for most three-dimensional biological modeling. However, these two modeling methods cannot show the details of complex biological models (Nie et al., 2020). ZBrush is a three-dimensional digital engraving software with powerful polygon data processing ability, and can process the details of complex curved surfaces. Therefore, ZBrush software was used to build a three-dimensional model of the hadal snailfish and its different tissues and organs. First, the main outline of the hadal snailfish body was established. The hadal snailfish was 180 mm long and 45 mm wide with a skin thickness of 1 mm. Then, according to the anatomical and scanning data of the hadal snailfish, the contour shapes of different tissues and organs were constructed, converted into a polygonal grid, and subjected to multi-stage subdivision, and the structures of various tissues and organs were more accurately carved out. Finally, the models of different tissues and organs were assembled to generate a three-dimensional model of the hadal snailfish (Figures 4C, D).

### Point cloud data processing

Because the generated 3D model of the hadal snailfish had some irregular surfaces, it would have affected the grid division, increased the calculation time, and reduced the calculation efficiency. Therefore, to ensure the anatomical geometric model, the point cloud data of each tissue and organ model of the hadal snailfish obtained from ZBrush was processed by Geomagic studio software (Figures 4E, F).

### Accurate surface processing

First, the point cloud was transformed into a polygon that could be manipulated and edited by an accurate surface. Contour lines were then manually built and edited, surface patches were built and repaired, and more contour lines in complex areas of the surface were controlled to ensure the integrity of the surface and make it easier to select mesh nodes during subsequent mesh division. It was checked whether there were any intersections or incorrect parts of the curved surfaces, and modifications ere made accordingly. Finally, the grating was constructed and the curved surface was fitted to obtain the solid geometric model of the hadal snailfish (Figures 4G, H).

## Quasi-static compression test

In this paper, we used *Harpadon nehereus* as the experimental sample, a near-benthic fish living within 50m of the seafloor. The *Harpadon nehereus* was first stored in a refrigerator at 4~6°C until the test was performed. The procedure of the quasi-static compression test is shown in Figure 5. Before testing, the *Harpadon nehereus* was removed from the refrigerator and placed in a water bath at room temperature of about 20°C for 10~15min to thaw. Thawed *Harpadon nehereus* heads, bodies, and tails are cut using stainless steel knives at room temperature. The specimen dimensions were measured after cutting, and the cut *Harpadon nehereus* specimens are shown in Figure 5A. A total of 27 specimens were obtained from different parts of the *Harpadon nehereus*, and three sets of tests were performed on different parts with loading rates of 25 mm/min, 50 mm/min, and 100 mm/min, and all experiments were done at room temperature (16-25°C). The experiments were repeated three times for the same part at the same speed to reduce the experimental error. Quasi-static compression test on different parts of fish using electronic universal tensile tester CMT-5105GL. The strain rate at each loading rate varies from 0.039-0.069 s-1, 0.079-0.117 s-1, and 0.145-0.235 s-1 due to the difference in the original spacing of each test sample, and the average value of the test data is taken as the test result at the loading rate, as shown in Figure 5B.

The fish stress-strain curve obtained from the quasi-static compression test is shown in Figure 6. In quasi-static compression experiments, by comparing the stress-strain relationships of soft tissue materials at three different strain rates, it was found that each material exhibited different degrees of strain rate effects, where the stresses in the head and tail at higher strain rates were greater than those at lower strain rates, while the stresses in the fish body at higher strain rates were less than those at lower strain rates, due to the more homogeneous and homogeneous tissue (fewer bones) in the fish body compared to the fish head, and thus the fish tissue was less resistant to compression under high strain rate conditions. The average values under each group of loading rates were calculated and summarized in Table 1. It can be seen that the elastic modulus, strength, and ultimate stress of the fish tail are greater than the values of the fish head and body, due to more fat and softer tissues in the fish body; the fish head tissue is not uniform, with slightly hard bones and soft brain tissue, etc.; the fish tail usually swings more and has good muscle elasticity. By

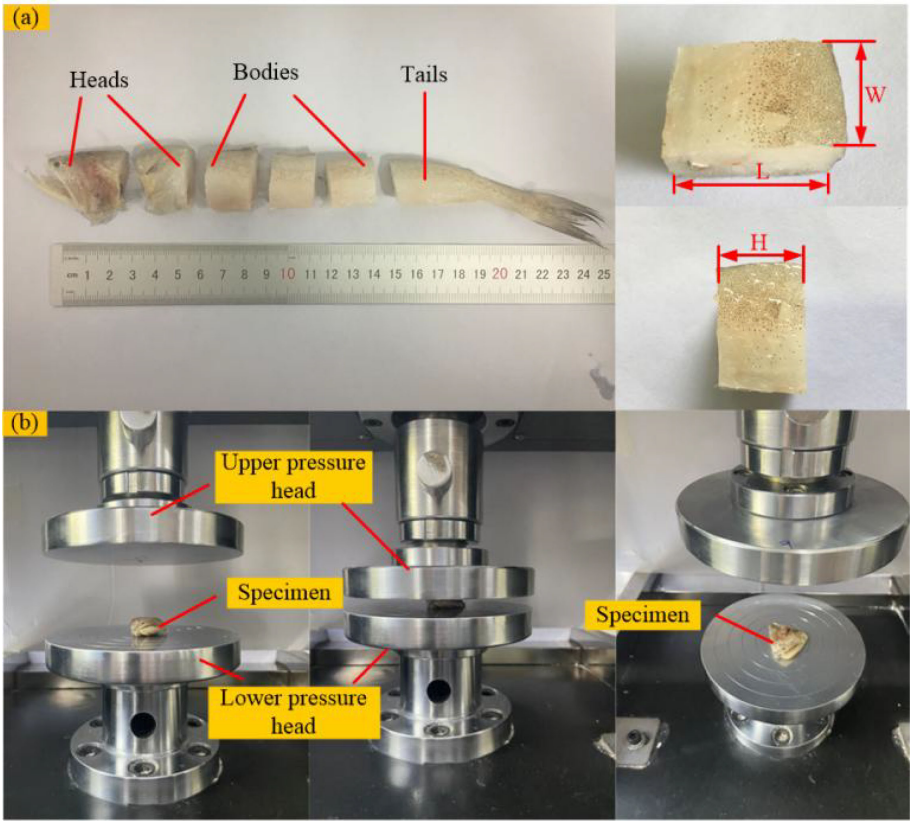


FIGURE 5
Quasi-static compression test **(A)** preparation of test samples of Harpadon nehereus; **(B)** quasi-static compression test of Harpadon nehereus.

comparing with the test results of Chen et al. (2011). and Zhou et al. (2010). the elastic modulus of the fish material obtained in this paper is smaller, with a difference of 0.5 MPa, which is also due to the relatively soft test sample.

## Finite element model of the hadal snailfish

As a pre-processing step of the finite element analysis of the hadal snailfish, model meshing was conducted to obtain the finite element analysis model. HyperMesh software was used to mesh the tissues and organs of the hadal snailfish, and a tetrahedral mesh was used to ensure uniform meshing. When capturing the hadal snailfish with the HSMPS, the movement of the fins is complicated. In the simulation, the finite element model of the fins was removed, and the vertebrae were simplified into a spine. The finite element model construction of the hadal snailfish was divided into the following steps. The geometric simplification of the tissues and organs of the hadal snailfish was respectively carried out. Then, 2D grid division was respectively carried out, the quality of the grid was checked, the unqualified grid was readjusted and divided, and a 3D solid grid was finally generated. The resulting grid division of the hadal snailfish is presented in Figure 7 and had 69,203 nodes and 425,660 units. The tissues and organs of the hadal snailfish were connected by common nodes, and normal contact was set between them. The contact type of the tissues and organs was defined as Automatic_singel_surface, and the dynamic and static friction coefficients were both set to 0.2.

The main research objective of this study is the dynamic response of different tissues and organs of the hadal snailfish during collision. Therefore, the possible collision position of the hadal snailfish was simplified, and a flat plate was used instead. The dimensions of the rectangular plate were 68 × 68 × 10 mm (length × width × height). The initial position of the hadal snailfish was located in the center of the flat plate at a distance of 0.1 mm from the plate. The initial velocity of the hadal snailfish was considered to always be along the normal direction of the flat plate. The finite element model of the hadal snailfish colliding with the flat plate is shown in Figure 8. When sucking the hadal snailfish *via* the HSMPS, the pumping speed is very high, which easily causes serious damage to the fish. However, if the pumping speed is too low, the fish can actively swim against the current,

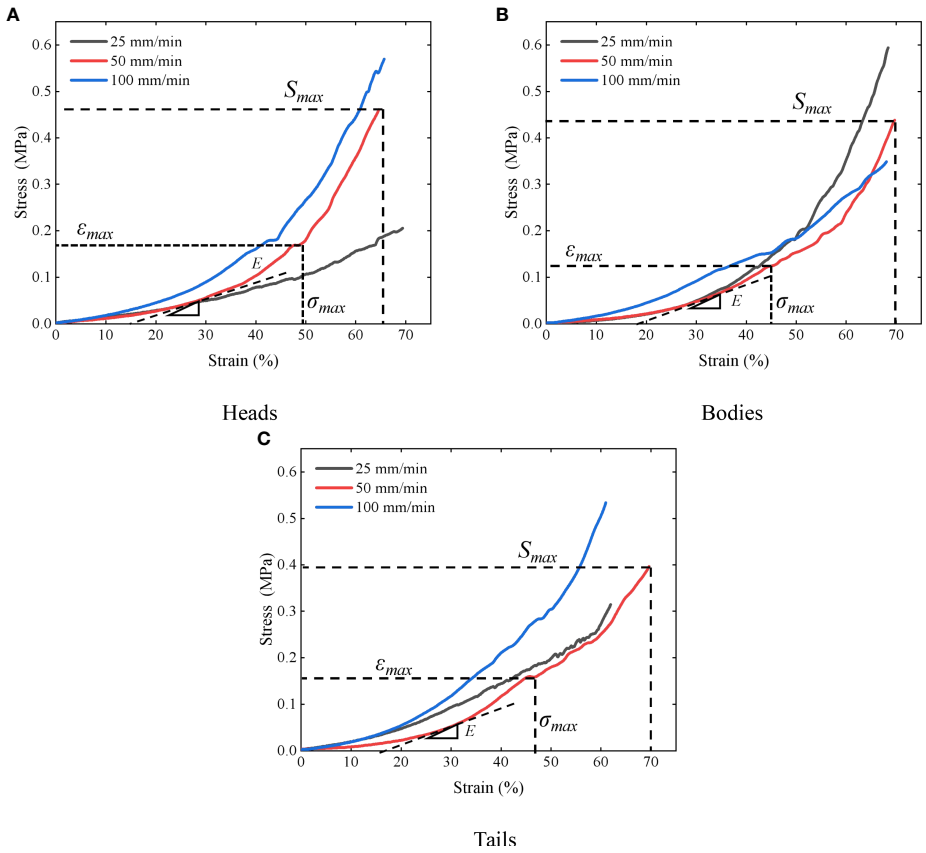


FIGURE 6
Stress-strain curves of different parts of the *Harpadon nehereus* **(A)** heads; **(B)** bodies; **(C)** tails.

resulting in the inability to capture the target. When the pumping speed is higher than the limit flow rate of the fish, the fish cannot continue to swim upstream, and the limit flow rate of the fish is in the range of 0.6-1.2 m/s (Long et al., 2016a, 2016b; Xu et al., 2018). In this study, four pump flows of 7.84 $m^3$/h (0.6 m/s), 10.45 $m^3$/h (0.8 m/s), 13.07 $m^3$/h (1.0 m/s), and 15.68 $m^3$/h (1.2 m/s) were selected to simulate and analyze the hadal snailfish collision process. The materials of the flat plates were defined as rubber material (SPDA, $\rho = 1.6$ g/$cm^3$, $E = 5$ MPa, $\mu = 0.47$) and titanium alloy material (PCPA, $\rho = 4.51$ g/$cm^3$, $E = 110000$ MPa, $\mu = 0.34$). The Lagrange method was used in the calculation of the collision of the hadal snailfish, and the penalty function method was used to solve the contact-collision algorithm. To more accurately obtain the acceleration of the hadal snailfish skull, five feature points on the skull were selected, and their positions were the front (a), top (b), right (c), bottom (d), and left (e). The motion, such as the movement and rotation of the upper and lower surfaces of the plate in three directions, was constrained to six degrees of freedom, and the simulation time was 10 ms. The contact between the hadal snailfish and the plate was defined as Automatic_surface_to_surface, and the friction coefficient was 0.2.

TABLE 1 Material parameters of different parts of the *Harpadon nehereus*.

| Parts | Elastic modulus | Compressive strength | Ultimate stress | Ultimate Strain |
|---|---|---|---|---|
| Heads | 0.61MPa | 0.20 | 0.15MPa | 46% |
| Bodies | 0.58MPa | 0.20 | 0.14MPa | 43% |
| Tails | 0.71MPa | 0.28 | 0.18MPa | 42% |

# Results and discussion

## Simulation analysis of the collision process

The history curve of each response and time in the collision process is shown in Figure 9. Figure 9A presents the stress-time curve when the hadal snailfish collided with the PCPA at a speed

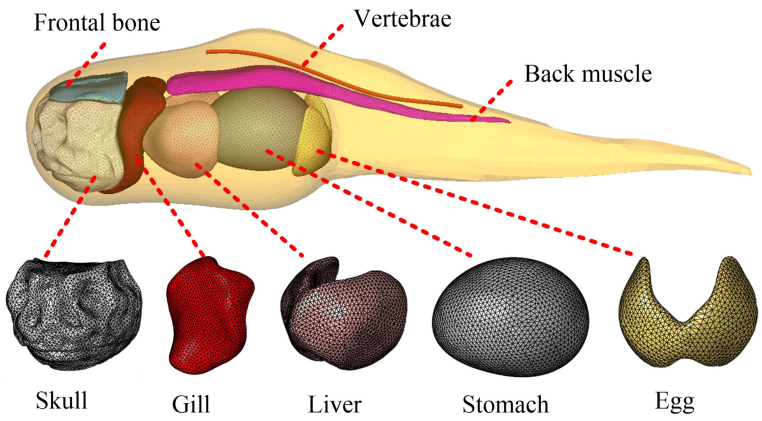


FIGURE 7
Finite element model of hadal snailfish.

of 1 m/s. The stress of the hadal snailfish began to increase after contacting the PCPA, and reached its peak at 1 ms. The stress of the hadal snailfish then gradually decreased from 1-2 ms, which was mainly because of the high rigidity of the PCPA and the rebound of the fish after contacting the PCPA. The stress tended to be stable from 2-10 ms until the end of collision. In the collision process, the maximum stress of hadal snailfish is greater than the ultimate stress $\epsilon_{max}$ and full compressive strength $S_{max}$.therefore, hadal snailfish in the collision PCPA easily cause damage. The strain-time curve is exhibited in Figure 9B. In the initial stage of collision, the hadal snailfish contacted the PCPA to produce deformation, and the strain increased with time. After 1 ms, the hadal snailfish began to rebound when its tissues and organs squeezed each other to produce stress fluctuations. The acceleration-time history curve of each characteristic point of the skull is shown in Figure 9C. In the initial stage of collision, the acceleration of the hadal snailfish skull reached its peak, namely 8*g*, after contacting the PCPA, after which the acceleration gradually decreased and finally tended to be stable. Sun et al. analyzed the process of a fish colliding with an axial pump. *Via* comparative analysis, the simulation results obtained in the present study were found to be basically consistent with the simulation and experimental results of Sun et al. (2020). This indicates that the finite element model

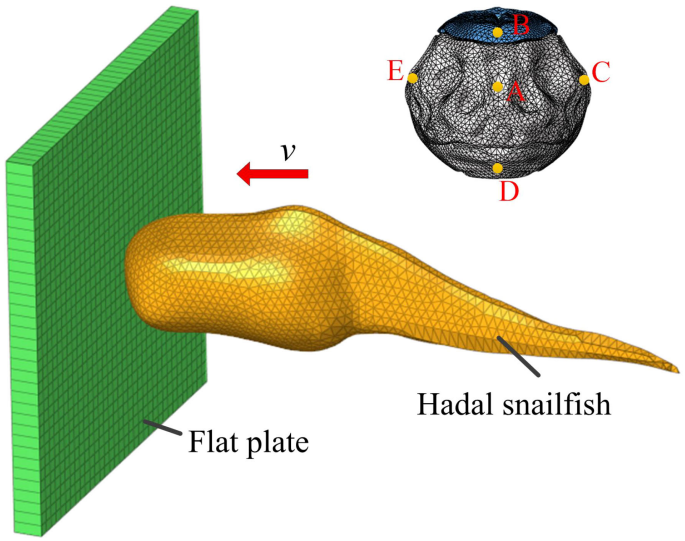


FIGURE 8
Simulation model of hadal snailfish collision.

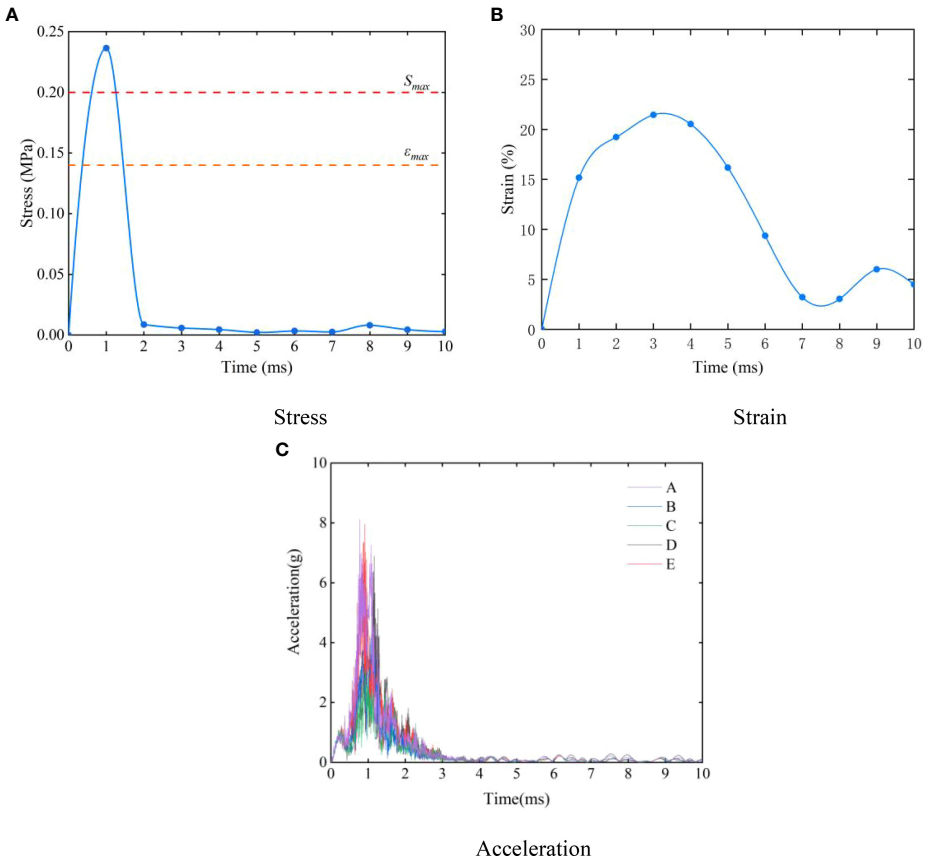


FIGURE 9
History curve of each response and time in collision process **(A)** stress; **(B)** strain; **(C)** acceleration.

of the hadal snailfish constructed in this study can better reflect the mechanical response of the hadal snailfish collision process.

## Stress and strain distributions of organs

Figure 10 exhibits the distributions of stress and strain in different tissues and organs during the collision of the hadal snailfish with the PCPA at 1 m/s. Among the hadal snailfish bones, the stress of the skull was the highest, followed by that of the frontal bone, and the stress of the vertebrae was the lowest. The stress of the skull was found to be concentrated at the contact position between the skull and the PCPA, and the maximum stress was 0.236MPa,which was greater than the ultimate stress of the material. Therefore, the skull of the hadal snailfish was the most vulnerable to damage during collision. The stress of the frontal bone was concentrated in the second half of the collision, and the maximum stress was 0.097 MPa. The stress distributions of the skull and frontal bone are shown in Figure 10(a). The strain distributions of the soft tissue are shown in Figure 10(b). During the collision of the soft tissue of the hadal snailfish, the strain of the liver was the highest. Moreover, the strain was concentrated on both sides, mainly *via* the squeezing of the stomach and gills, and the maximum strain was 9.2%; this was found to be the most likely strain to cause damage during the collision. The strain of the stomach was concentrated on the left and right sides, and the maximum strain was 7.9%. The strain of the gills was concentrated in the middle position, and the maximum strain was 4.7%. The strain of the eggs was found to be the lowest with a maximum value of 2.3%. The eggs are located behind the fish body, and they were mainly strained by stomach squeezing. Therefore, the possibility of the eggs being damaged during collision was found to be the lowest.

## Results of numerical analysis at the collision speed

The response curves of various tissues and organs at different collision speeds are shown in Figure 11. Figure 11A presents the maximum stress curve of the hadal snailfish during the process of colliding with the PCPA at different speeds. With the increase

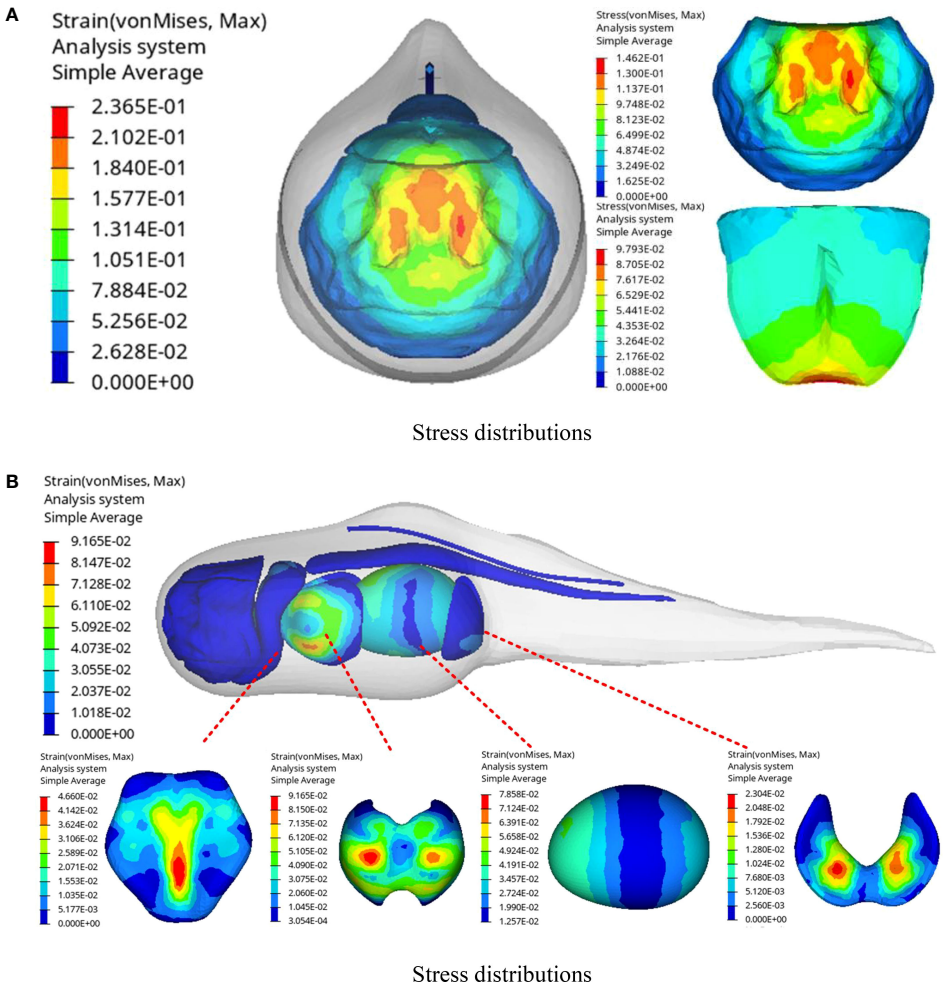


FIGURE 10
Stress and strain distribution of hadal snailfish during collision **(A)** stress distributions; **(B)** strain distributions.

of the speed, the stress of the skull, frontal bone, and vertebrae increased continuously. At the collision speed of 1.2 m/s, the maximum stress was 0.24 MPa, which was 1.2 times the stress at the collision speed of 0.6 m/s. Figure 11B shows the maximum strain curve of the hadal snailfish colliding with the PCPA at different speeds, from which it is evident that the strains of the liver and stomach were found to be higher. At the collision speed of 1.2 m/s, the maximum strain of the liver was 115%, which was 1.63 times the strain at the collision speed of 0.6 m/s. Figure 11C exhibits the acceleration of the skull when the hadal snailfish collided with the PCPA at different speeds. It can be seen from the figure that the acceleration of point A was the highest, mainly because point A was in direct contact with the PCPA during the collision of the skull. Moreover, the acceleration of point C was the same as that of point E, mainly because points C and E were symmetrically distributed on both sides of the skull, and the acceleration of point D was the lowest. At the collision speed of 1.2 m/s, the acceleration of point A was 12.4*g*, which was 3.35 times that at the collision speed of 0.6 m/s. The skull and liver of the hadal snail are easily damaged at high collision speeds. Therefore, while ensuring that the hadal snailfish can be sucked into the HSMPS, the flow rate of the suction pump should be reduced to the greatest extent.

## Results of numerical analysis at the collision position

The response curves of various tissues and organs under different collision positions are shown in Figure 12. Figure 12A presents the stress curve of the skull when the hadal snailfish collided with different materials at a speed of 1 m/s. During the process of the hadal snailfish colliding with the PCPA, the stress of the skull reached the maximum at the initial stage of collision,

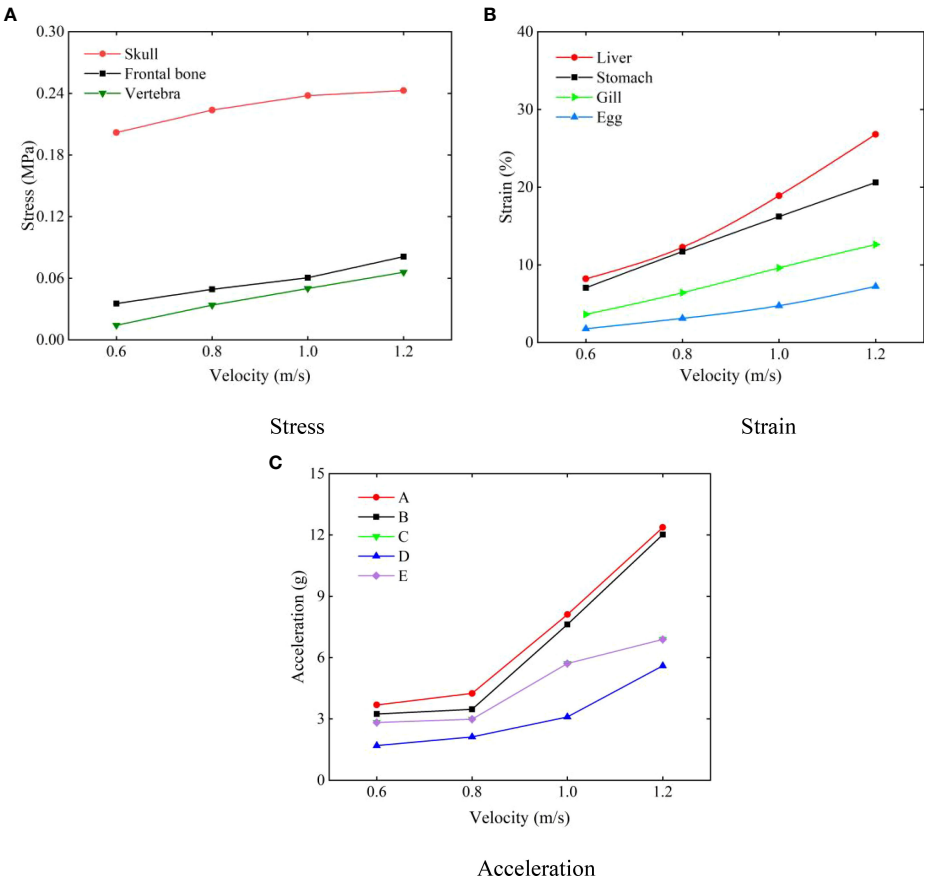


FIGURE 11
Response curves of various tissues and organs at different collision speeds **(A)** stress; **(B)** strain; **(C)** acceleration.

and then tended to be stable until the end of collision. During the process of the hadal snailfish colliding with the SPDA, the stress value of the skull reached the first peak at the initial stage of collision. With the continuation of time, the hadal snailfish continued to collide with the SPDA. Because the SPDA had elasticity, it was found to play a buffering role in the collision of the hadal snailfish, and the speed of the fish decreased. At this time, the maximum stress decreased with time. The hadal snailfish rebounded in 5 ms, and the stress reached the maximum value at this time. After that, the maximum stress of the skull decreased with the continuation of time until the end of collision. When the hadal snailfish collided with PCPA, the maximum stress of the skull was 2.95 times that when the fish collided with the SPDA. Figure 12B presents the strain curve of the liver when the hadal snailfish collided with different materials at a speed of 1 m/s. When the hadal snailfish collided with the PCPA, the stress of the liver fluctuated greatly, and the tissues and organs were squeezed violently during the collision. The maximum strain of the liver when colliding with the PCPA was 2.26 times that when colliding with the SPDA. Figure 12C shows the acceleration of the skull when the hadal snailfish collided with the SPDA at a speed of 1 m/s. When the hadal snailfish collided with PCPA, the acceleration at point A was 2.5 times that when it collided with the SPDA. The response values (stress, strain, acceleration) of different tissues and organs were high when the hadal snailfish collided with the PCPA. Therefore, to reduce the possibility of damage to the hadal snailfish during the suction process, a layer of buffer material can be coated on the inner wall of the HSMPS.

Figure 12 shows that deep-sea organisms are prone to collide with PCPA and cause damage during capture. To minimize the damage, we installed a layer of polyurethane open-cell foam ($\rho$ = 1.05 g/cm$^3$, $E$ = 8 MPa, $\mu$ = 0.47)in the PCPA. Figure 13 shows the stress-time curves when the hadal snailfish collided with PCPA at different velocities. When the hadal snailfish collided with PCPA at 1 m/s, the maximum stress value of the hadal snailfish was 0.148 MPa when there was foam material, while the stress value was 0.236 MPa when there was no foam material, and the stress value of the hadal snailfish was reduced. The maximum stress value of hadal snailfish is less than the

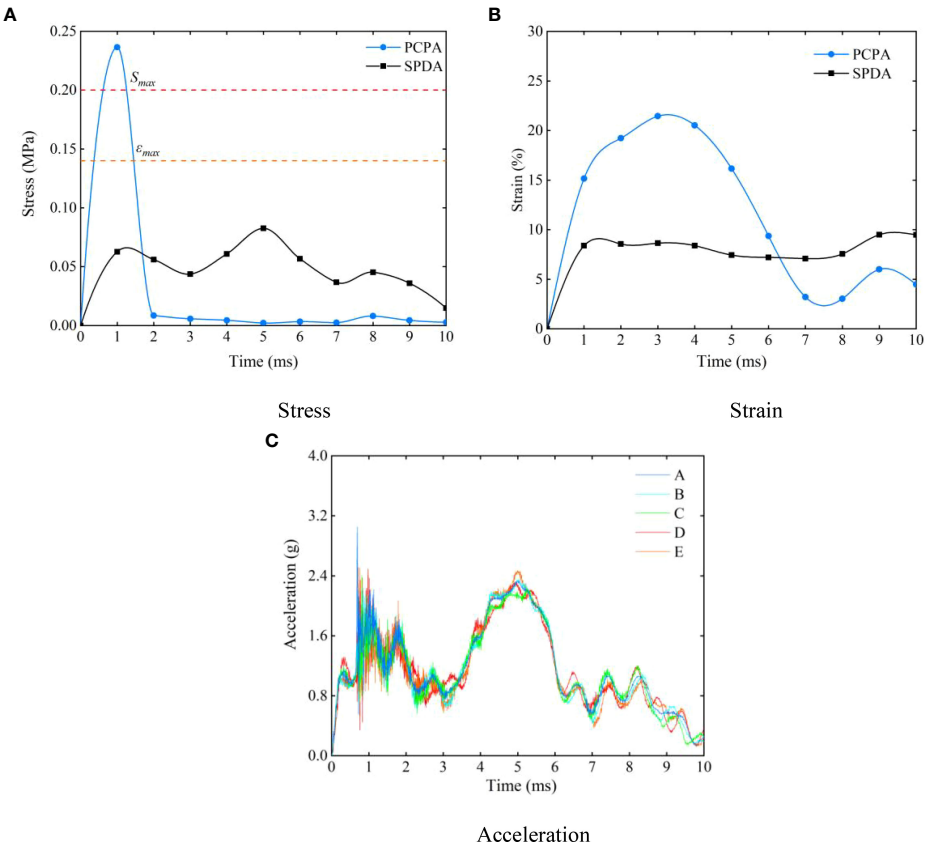


FIGURE 12
Response curves of various tissues and organs under different collision position **(A)** stress; **(B)** strain; **(C)** acceleration.

material's compressive strength. Still, when the collision speed is more significant than 0.8m/s, the maximum stress of hadal snailfish is greater than the ultimate stress of the material, and damage may occur when hadal snailfish collide with PCPA. Therefore, to capture deep-sea biological samples while reducing damage to marine organisms, the flow rate of the suction pump should be adjusted in the range of 131 L/min~174 L/min.

## Conclusion and perspectives

Obtaining biological samples *in situ* in the deep sea has become a significant concern for the scientific community. At present, deep-sea biological samplers are mainly carried on landers or deep submersibles. The biological collection is carried out by passive trapping, which has a random nature and may not capture seafloor organisms in one dive. Therefore, we propose a pumping sampling method of deep-sea organisms, which realizes active sampling of deep-sea organisms by controlling the flow rate of the pump, designs a pressure compensation mechanism to compensate for the pressure drop in the recovery process of the sampler, and uses thermal insulation materials to realize the low-temperature environment inside the sampler.

Apart from collecting samples and maintaining them *in situ* conditions, we have also researched the low damage of the sampler capture process of deep-sea organisms. Due to the unique living environment of deep-sea organisms, the laboratory cannot analyze their dynamic response during capture. Therefore, we established a three-dimensional model of deep-sea gelatinous fish and performed quasi-static compression tests on different parts of the seafloor gelatinous fish to obtain a numerical analysis model of marine gelatinous fish, which can be used for impact biomechanics, biomedical and bionomics applications.

We analyzed the influence of different structural parameters of the HSMPS on the tissues and organs of gelatinous fish. The results showed that when gelatinous fish collided with PCPA, the stress of the skull was greater than the ultimate stress and compressive strength of the material, and gelatinous fish might be damaged. We installed a layer of polyurethane open-cell foam in PCPA. The analysis shows that polyurethane open-cell foam can effectively reduce the stress value of gelatinous fish during a collision. When

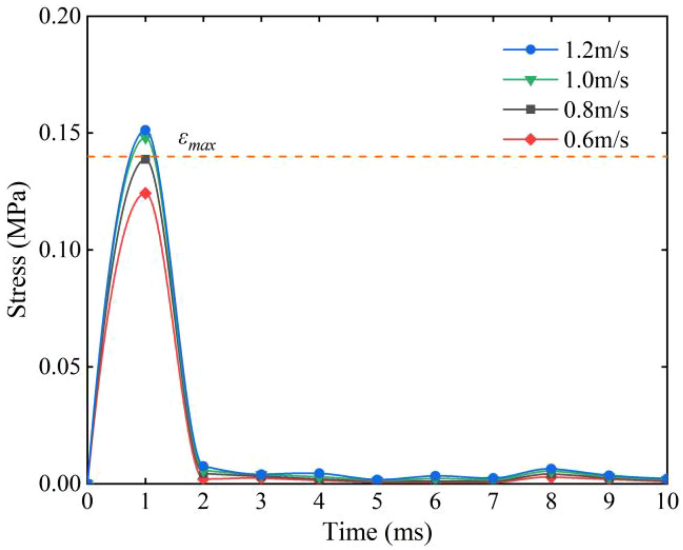


FIGURE 13
Response curves of deep-sea organisms at different collision speeds.

the collision speed of gelatinous fish is less than 0.8m/s, the stress of their skulls is less than the material's ultimate stress and compressive strength. Therefore, we control the pump's flow rate in the range of 131 L/min to 174 L/min to balance the biological damage and escape speed in the deep sea.

The pressure retention and insulation tests proposed in this study have been verified in the laboratory. In our future research, we will design a deep-sea biological sampling-transfer-culture system to put biological samples from deep-sea *in situ* into laboratory culture and analyze the influencing factors affecting marine biological activity to reveal the patterns of different factors on marine biological activity.

## Data availability statement

The raw data supporting the conclusions of this article will be made available by the authors, without undue reservation.

## Author contributions

GL and YJ wrote the initial draft and coordinated the drafting of the paper, and participated in the experimental design. YP, DL, and BW provided ideas on manuscript writing. All authors contributed to the article and approved the submitted version.

## Funding

This work was supported by the National Key Research and Development Program of China (Grant No. 2016YFC0300502) and Postgraduate Scientific Research Innovation Project of Hunan Province (Grant No. CX20210985). It was also supported by Special project for the construction of innovative provinces in Hunan (Grant No. 2020GK1021, 2019SK2271, 2019GK1010, 2019GK1012).

## Conflict of interest

The authors declare that the research was conducted in the absence of any commercial or financial relationships that could be construed as a potential conflict of interest.

## Publisher's note

All claims expressed in this article are solely those of the authors and do not necessarily represent those of their affiliated organizations, or those of the publisher, the editors and the reviewers. Any product that may be evaluated in this article, or claim that may be made by its manufacturer, is not guaranteed or endorsed by the publisher.

# References


Billings, A., Kaiser, C., Young, C. M., Hiebert, L. S., Cole, E., Wagner, J. K., et al. (2017). SyPRID sampler: A large-volume, high-resolution, autonomous, deep-ocean precision plankton sampling system. *Deep Sea Res. Part II: Topical Stud. Oceanog* 137, 297–306. doi: 10.1016/j.dsr2.2016.05.007

Caron, J., Price, J. S., and Rochefort, L. (2015). Physical properties of organic soil: Adapting mineral soil concepts to horticultural growing media and histosol characterization. *Vadose Zone J.* 14 (6), 369–379. doi: 10.2136/vzj2014.10.0146

Chen, M., Jia, L. B., and Yin, X. Z. (2011). Relaxation modulus of caudal fin studied by fractional zener model. *Chin. J. Theor. Appl. Mechanics.* 43 (1), 217–220. doi: 10.6052/0459-1879-2011-1-lxxb2010-145

Clark, M. R., Consalvey, M., and Rowden, A. A. (2016). *Biological sampling in the deep sea* (New Jersey: John Wiley & Sons, Inc).

Edgcomb, V. P., Taylor, C., Pachiadaki, M. G., Honjo, S., Engstrom, I, and Yakimov, M.. (2016). Comparison of Niskin vs. *in situ* approaches for analysis of gene expression in deep Mediterranean Sea water samples. Deep-sea research, Part II. *Topical studies in oceanography* 129, 213–222. doi: 0.1016/j.dsr2.2014.10.020

Feng, J. C., Liang, J. Z., Zhang, S., Yang, Z.F., and Zhu, Z.C.. (2020). Development of deep-Sea biological resources exploitation equipment. *Strategic Study CAE.* 22 (6), 67–75. doi: 10.15302/J-SSCAE-2020.06.009

Garel, M., Bonin, P., Martini, S., Guasco, S., Roumagnac, M., Bhairy, N., et al. (2019). Pressure-retaining sampler and high-pressure systems to study deep-sea microbes under *in situ* conditions. *Front. Microbiol.* 10, 453. doi: 10.3389/fmicb.2019.00453

Gerringer, M. E., Drazen, J. C., Linley, T. D., Summers, A. P., Jamieson, A. J., and Yancey, P. H.. (2017). Distribution, composition and functions of gelatinous tissues in deep-sea fishes. *R. Soc. Open Science.* 4 (12), 171063. doi: 10.1098/rsos.171063

Jamieson, A. J., Fujii, T., Mayor, D. J., Solan, M., and Priede, I. G.. (2010). Hadal trenches: the ecology of the deepest places on earth. *Trends Ecol. Evolution.* 25 (3), 190–197. doi: 10.1016/j.tree.2009.09.009

Linley, T. D., Gerringer, M. E., Yancey, P. H., Drazen, J. C., Weinstock, C. L., and Jamieson, A. J.. (2016). Fishes of the hadal zone including new species, *in situ* observations and depth records of liparidae. *Deep sea Res. Part I: oceanog Res. papers.* 114, 99–110. doi: 10.1016/j.dsr.2016.05.003

Linley, T. D., Lavaleye, M., Maiorano, P., Bergman, M., Capezzuto, F., Cousins, N. J., et al. (2017). Effects of cold-water corals on fish diversity and density (European continental margin: Arctic, NE Atlantic and Mediterranean sea): Data from three baited lander systems. *Deep Sea Res. Part II: Topical Stud. Oceanog* 145, 8–21. doi: 10.1016/j.dsr2.2015.12.003

Long, X., Xu, M., Lyu, Q., and Zou, J. (2016a). Impact of the internal flow in a jet fish pump on the fish. *Ocean Engineering.* 126 (nov.1), 313–320. doi: 10.1016/j.oceaneng.2016.09.027

Long, X., Zhang, J., Wang, Q., Xiao, L., Xu, M., Lyu, Q., et al. (2016b). Experimental investigation on the performance of jet pump cavitation reactor at different area ratios. *Exp. Thermal Fluid Science.* 78, 309–321. doi: 10.1016/j.expthermflusci.2016.06.018

Nie, F. Y., Xie, H., and Li, P. (2020). Research on digitalization method of 3D entity based on zbrush technology. *Comput. Inf. Technol* 28 (06), 16–17. doi: 10.19414/j.cnki.1005-1228.2020.06.006

Orr, J. W. (2020). A new snailfish of the genus careproctus (Cottiformes: Liparidae) from the Beaufort Sea. *Copeia.* 108 (4), 815–819. doi: 10.1643/CI2020089

Peoples, L. M., Norenberg, M., Price, D., McGoldrick, M., Novotny, M., Bochdansky, A., et al. (2019). A full-ocean-depth rated modular lander and pressure-retaining sampler capable of collecting hadal-endemic microbes under *in situ* conditions. *Deep Sea Res. Part I: Oceanog Res. Papers.* 143, 50–57. doi: 10.1016/j.dsr.2018.11.010

Phillips, B. T., Becker, K. P., Kurumaya, S., Galloway, K. C., Whittredge, G., Vogt, D. M., et al. (2019). A dexterous, glove-based teleoperable low-power soft robotic arm for delicate deep-sea biological exploration. *Sci. Rep.* 8 (1), 1–9. doi: 10.1038/s41598-018-33138-y

Ramirez-Llodra, E., Brandt, A., Danovaro, R., De Mol, B., Escobar, E., German, C. R., et al. (2010). Deep, diverse and definitely different: unique attributes of the world's largest ecosystem. *Biogeosciences.* 7 (9), 2851–2899. doi: 10.5194/bg-7-2851-2010

Sun, Z. K., Pan, Q., Zhang, D.S., and Shi, W.D. (2020). *Research on fish damage mechanism of axial flow pump based on CFD-DEM coupling method* (Jiangsu university). doi: 10.16076/j.cnki.cjhd.2020.05.011

Sun, Z. K., Pan, Q., Zhang, D. S., et al. (2020). Study on fish damage mechanism in axial-flow pump based on the CFD-DEM coupling method. *Chin. J. Hydrodynamics.* 35 (5), 631–639.

Vogt, D. M., Becker, K. P., Phillips, B. T., Graule, M. A., Rotjan, R. D., Shank, T. M., et al. (2018). Shipboard design and fabrication of custom 3D-printed soft robotic manipulators for the investigation of delicate deep-sea organisms. *PloS One* 13 (8), e0200386. doi: 10.1371/journal.pone.0200386

Wang, H., Chen, J., Wang, Y., Fang, J., and Fang, Y.. (2020). Research and analysis of pressure-maintaining trapping instrument for macro-organisms in hadal trenches. *J. Mar. Sci. Engineering.* 8 (8), 596. doi: 10.3390/jmse8080596

Wang, K., Shen, Y., Yang, Y., Gan, X., Liu, G., Hu, K., et al. (2019). Morphology and genome of a snailfish from the Mariana trench provide insights into deep-sea adaptation. *Nat. Ecol. evolution.* 3 (5), 823–833. doi: 10.1038/s41559-019-0864-8

Xu, M. S., Yang, X. L., Long, X. P., Lyu, Q., and Ji, B. (2018). Numerical investigation of turbulent flow coherent structures in annular jet pumps using the LES method. *Sci. China Technolog Sci.* 61 (1), 86–97. doi: 10.1007/s11431-017-9047-8

Yancey, P. H., Gerringer, M. E., Drazen, J. C., Rowden, A. A., and Jamieson, A.. (2014). Marine fish may be biochemically constrained from inhabiting the deepest ocean depths. *Proc. Natl. Acad. Sci.* 111 (12), 4461–4465. doi: 10.1073/pnas.1322003111

Zhou, M., Yin, X. Z., and Tong, B. G. (2010). Study of skin and muscle mechanical properties of crucian carp (Carassius auratus). *J. Exp. Mechanics.* 25 (5), 536–545. doi: 10.3788/HPLPB20102208.1731